JYX
JYVÄSKYLÄN YLIOPISTO
UNIVERSITY OF JYVÄSKYLÄ

This is a self-archived version of an original article. This version may differ from the original in pagination and typographic details.

Author(s): Jokiniemi, L.; Suhonen, J.

Title: Muon-capture strength functions in intermediate nuclei of 0νββ decays

Year: 2019

Version: Published version

Copyright: © 2019 American Physical Society

Rights: In Copyright

Rights url: http://rightsstatements.org/page/InC/1.0/?language=en

Please cite the original version:

Jokiniemi, L., & Suhonen, J. (2019). Muon-capture strength functions in intermediate nuclei of 0νββ decays. Physical Review C, 100(1), Article 014619.
https://doi.org/10.1103/PhysRevC.100.014619

Muon-capture strength functions in intermediate nuclei of $0\nu\beta\beta$ decays

L. Jokiniemi and J. Suhonen
University of Jyväskylä, Department of Physics, P.O. Box 35 (YFL), FI-40014, Finland

(Received 22 May 2019; published 31 July 2019)

Capture rates of ordinary muon capture (OMC) to the intermediate nuclei of neutrinoless double beta ($0\nu\beta\beta$) decays of current experimental interest are computed. The corresponding OMC (capture-rate) strength functions have been analyzed in terms of multipole decompositions. The computed low-energy OMC-rate distribution to ^{76}As is compared with the available data of Zinatulina *et al.* [Phys. Rev. C **99**, 024327 (2019)]. The present OMC computations are performed using the Morita-Fujii formalism by extending the original formalism beyond the leading order. The participant nuclear wave functions are obtained in extended no-core single-particle model spaces using the spherical version of proton-neutron quasiparticle random-phase approximation (pnQRPA) with two-nucleon interactions based on the Bonn one-boson-exchange G matrix. The Hamiltonian parameters are taken from our earlier work [Jokiniemi *et al.*, Phys. Rev. C **98**, 024608 (2018)], except for $A = 82$ nuclei for which the parameters were determined in this work. Both the OMC and $0\nu\beta\beta$ decays involve momentum exchanges of the order of 100 MeV and thus future measurements of the OMC strength functions for $0\nu\beta\beta$ daughter nuclei help trace the in-medium renormalization of the weak axial couplings with the aim to improve the accuracy of the $0\nu\beta\beta$-decay nuclear matrix elements.

DOI: 10.1103/PhysRevC.100.014619

I. INTRODUCTION

Ordinary muon capture (OMC) is a process in which a negative muon implanted in an atomic K orbit is captured by the nucleus of the atom. The large momentum, $q \approx 50$–100 MeV, exchanged in the process leads to final states that are both highly excited and of high multipolarity, quite like in the case of the neutrinoless double beta ($0\nu\beta\beta$) decay. In this way the OMC corresponds to the right branch (β^+ type of transitions) of the $0\nu\beta\beta$ virtual transitions, which makes it a promising tool to study the nuclear matrix elements (NMEs) of the $0\nu\beta\beta$ decay [1,2], as also the neutrino-nucleus interactions in general [3]. In particular, the OMC probes nuclear responses for medium-energy astro-(anti)neutrinos (μ and τ (anti)neutrinos from supernovae) [3,4].

The muon-capture processes concern β^+ type of transitions from a mother nucleus ${}^{A}_{Z}X$ to the states of the residual nucleus ${}^{A}_{Z-1}Y$ (see the review [5]). Over years nuclear-structure calculations for the OMC transitions have been performed in a wide range of nuclear masses in order to probe the right-leg (the β^+ side) virtual transitions of $0\nu\beta\beta$ decays and the value of the particle-particle parameter $g_{\rm pp}$ of the proton-neutron quasiparticle random-phase approximation (pnQRPA), as discussed in Refs. [6–8], or the in-medium renormalization of the axial-vector coupling constant $g_{\rm A}$ [9–14]. The large momentum exchange involved in the OMC activates the induced weak currents, including the weak magnetism and pseudoscalar contributions, quite like in the case of the $0\nu\beta\beta$ decay [15]. The magnitude of the induced pseudoscalar term is largely unknown in finite atomic nuclei [9,10,16–23].

The OMC process we are interested in here can be written as

$$\mu^- + {}^{A}_{Z}\mathrm{X}(0^+) \rightarrow \nu_\mu + {}^{A}_{Z-1}\mathrm{Y}(J^\pi), \tag{1}$$

where the muon (μ^-) is captured by the 0^+ ground state of the even-even nucleus X of mass number A and atomic number Z leading to the J^π multipole states of its odd-odd isobar Y of atomic number $Z-1$; here J is the angular momentum and π the parity of the final state. At the same time a muon neutrino ν_μ is emitted. The capture rates to the full set of final states constitutes the OMC strength function.

In this study we compute the OMC strength functions in the intermediate nuclei of $0\nu\beta\beta$ decays up to some 50 MeV using the pnQRPA formalism. The strength function is composed of OMC rates to individual final states of multipolarities J^π, extending the idea of (n,p) charge-exchange reactions, which populate the 1^+ final states, thus producing the Gamow-Teller strength function. The OMC strength function can contain giant resonances analogously to the Gamow-Teller giant resonance [24] or the isovector spin-monopole [25,26] and higher isovector spin-multipole resonances [3,4,27,28]. Here we study the possible existence and structure of these resonances. In our earlier study [29] we computed the strength function for the OMC on ^{100}Mo and compared it with the available data [30]. In this study we extend those calculations by computing the strength functions for the OMCs on ^{76}Se, ^{82}Kr, ^{96}Mo, ^{100}Ru, ^{116}Sn, ^{128}Xe, ^{130}Xe, and ^{136}Ba, leading to states in $0\nu\beta\beta$ intermediate nuclei ^{76}As, ^{82}Br, ^{96}Nb, ^{100}Tc, ^{116}In, ^{128}I, ^{130}I, and ^{136}Cs. In the case of the OMCs on ^{76}Se we compare the low-energy part of our results with the recently available data from Zinatulina *et al.* [2].

Since the nuclei of interest are medium-heavy or heavy open-shell nuclei, the shell-model framework is unfeasible for the calculation of the strength functions due to the excessive computational burden and the very restricted single-particle model spaces allowed by the shell-model treatment. The pnQRPA formalism allows us to study the OMC strength

 ©2019 American Physical Society

functions at high energies, since it allows the use of large no-core single-particle bases. Even though the pnQRPA often fails to predict the properties of individual states accurately, it can reproduce the gross features of a distribution of nuclear states quite reasonably. It has been shown that the pnQRPA reproduces the locations of the isovector spin-dipole giant resonances reliably [31], and in our earlier OMC study it was shown that it also reproduces the location of the newly discovered OMC giant resonance correctly in the case of ^{100}Mo [29,30].

Additional OMC experiments and calculations concerning nuclei involved in $0\nu\beta\beta$ decays could help theories better evaluate the NMEs associated with the $0\nu\beta\beta$ decays and also the NMEs related to astro-(anti)neutrino interactions. Furthermore, the effective values of the axial-vector coupling $g_{\rm A}$ and induced pseudoscalar coupling $g_{\rm P}$ are involved both in $0\nu\beta\beta$ decays and in the OMC [32].

This paper is organized as follows. In Sec. II we briefly introduce the underlying formalism of the ordinary muon capture. In Sec. III we briefly discuss the determination of the model parameters. There we display and discuss the obtained results for the OMC rates and compare them with the available experimental data. The final conclusions are drawn in Sec. IV.

II. COMPUTATIONAL SCHEME

In this section we introduce briefly our computational scheme. The calculations are based on the pnQRPA theory. In Sec. II A we introduce the theoretical aspects of the OMC rate. The pnQRPA theory is explained briefly in Sec. II B.

A. Formalism of the ordinary muon capture

For the calculation of the OMC rates we use the robust formalism that was developed by Morita and Fujii in Ref. [33].

The muon capture rate to a J^π final state is written as

$$W = 8\left(\frac{Z_{\rm eff}}{Z}\right)^4 P(\alpha Z m'_\mu)^3 \frac{2J_f+1}{2J_i+1}\left(1-\frac{q}{m_\mu+AM}\right)q^2, \tag{2}$$

where A indicates the mass number of the initial and final nuclei, J_i (J_f) the angular momentum of the initial (final) nucleus, M the average nucleon rest mass, m_μ the bound muon mass (the rest mass of a muon minus the binding energy of the muon in the K orbital of the μ-mesonic atom), m'_μ the reduced mass of the muon in the parent μ-mesonic atom, Z the atomic number of the initial nucleus, α the fine-structure constant and q the exchanged momentum between the captured muon and the nucleus [33], i.e. the Q value of the OMC.

For heavy nuclei the capture rate has to be corrected for the muonic screening since the atomic orbit of the muon penetrates the nucleus. We follow the Primakoff method [34] correcting the capture rate by the factor $(Z_{\rm eff}/Z)^4$, where the effective atomic number $Z_{\rm eff}$ is obtained from the work of Ford and Wills [35]. The effective atomic numbers for the nuclei of interest are listed in the following section.

The Q value of the OMC process can be obtained from

$$q = (m_\mu - W_0)\left(1-\frac{m_\mu - W_0}{2(M_f+m_\mu)}\right), \tag{3}$$

where $W_0 = M_f - M_i + m_e + E_X$ [33]. Here M_f and M_i are the nuclear masses of the final and initial nuclei, m_e the rest mass of an electron and E_X the excitation energy of the final-state nucleus.

The term P in Eq. (2) can be written as

$$\begin{aligned} P = \frac{1}{2}\sum_{\kappa u}\Bigg| & g_{\rm V}\mathcal{M}[0\,l\,u]S_{0u}(\kappa)\delta_{lu} + g_{\rm A}\mathcal{M}[1\,l\,u]S_{1u}(\kappa) - \frac{g_{\rm V}}{M}\mathcal{M}[1\,\bar{l}\,u\,p]S'_{1u}(-\kappa) \\ & + \sqrt{3}\frac{g_{\rm V}q}{2M}\left(\sqrt{\frac{\bar{l}+1}{2\bar{l}+3}}\mathcal{M}[0\,\bar{l}+1\,u+]\delta_{\bar{l}+1,u} + \sqrt{\frac{\bar{l}}{2\bar{l}-1}}\mathcal{M}[0\,\bar{l}-1\,u-]\delta_{\bar{l}-1,u}\right)S'_{1u}(-\kappa) \\ & + \sqrt{\frac{3}{2}}\left(\frac{g_{\rm V}q}{M}\right)(1+\mu_p-\mu_n)(\sqrt{\bar{l}+1}W(1\,1\,u\,\bar{l};1\,\bar{l}+1)\mathcal{M}[1\,\bar{l}+1\,u+] \\ & + \sqrt{\bar{l}}W(1\,1\,u\,\bar{l};1\,\bar{l}-1)\mathcal{M}[1\,\bar{l}-1\,u-])S'_{1u}(-\kappa) - \left(\frac{g_{\rm A}}{M}\right)\mathcal{M}[0\,\bar{l}\,u\,p]S'_{0u}(-\kappa)\delta_{\bar{l}u} \\ & + \sqrt{\frac{1}{3}}(g_{\rm P}-g_{\rm A})\left(\frac{q}{2M}\right)\left(\sqrt{\frac{\bar{l}+1}{2\bar{l}+1}}\mathcal{M}[1\,\bar{l}+1\,u+] + \sqrt{\frac{\bar{l}}{2\bar{l}+1}}\mathcal{M}[1\,\bar{l}-1\,u-]\right)S'_{0u}(-\kappa)\delta_{\bar{l}u}\Bigg|^2, \end{aligned} \tag{4}$$

where $W(\ldots)$ are the usual Racah coefficients and $\mathcal{M}[k\,w\,u\,(\frac{\pm}{p})]$ nuclear matrix elements of the OMC. The NMEs $\mathcal{M}[k\,w\,u\,(\pm)]$ are dimensionless numbers while the NMEs $\mathcal{M}[k\,w\,u\,p]$ are related to the nucleon momentum and hence are in energy units. The matrix elements are defined in the following manner:

$$\int \Psi_{J_fM_f}\sum_{s=1}^{A} e^{-\alpha Z m'_\mu r_s} O_s \tau_-^s \Psi_{J_iM_i} d\mathbf{r}_1 \ldots d\mathbf{r}_A = \mathcal{M}\left[k\,w\,u\left(\frac{\pm}{p}\right)\right](J_i\,M_i\,u\,M_f - M_i|J_f\,M_f), \tag{5}$$

where $\Psi_{J_fM_f}$ ($\Psi_{J_iM_i}$) is the final (initial) nuclear wave function. The definition for the operator O_s can be found in Table I.

TABLE I. Definition of O_s in Eq. (5) for different nuclear matrix elements (NMEs).

NME	O_s
$\mathcal{M}[0\,w\,u]$	$j_w(qr_s)\mathcal{Y}^{M_f-M_i}_{0wu}(\hat{\mathbf{r}}_s)\delta_{wu}$
$\mathcal{M}[1\,w\,u]$	$j_w(qr_s)\mathcal{Y}^{M_f-M_i}_{1wu}(\hat{\mathbf{r}}_s,\boldsymbol{\sigma}_s)$
$\mathcal{M}[0\,w\,u\pm]$	$[j_w(qr_s)\pm\alpha Z(m'_\mu/p_\nu)j_{w\mp1}(qr_s)]\mathcal{Y}^{M_f-M_i}_{0wu}(\hat{\mathbf{r}}_s)\delta_{wu}$
$\mathcal{M}[1\,w\,u\pm]$	$[j_w(qr_s)\pm\alpha Z(m'_\mu/p_\nu)j_{w\mp1}(qr_s)]\mathcal{Y}^{M_f-M_i}_{1wu}(\hat{\mathbf{r}}_s,\boldsymbol{\sigma}_s)$
$\mathcal{M}[0\,w\,u\,p]$	$ij_w(qr_s)\mathcal{Y}^{M_f-M_i}_{0wu}(\hat{\mathbf{r}}_s)\boldsymbol{\sigma}_s\cdot\mathbf{p}_s\delta_{wu}$
$\mathcal{M}[1\,w\,u\,p]$	$ij_w(qr_s)\mathcal{Y}^{M_f-M_i}_{1wu}(\hat{\mathbf{r}}_s,\mathbf{p}_s)$

The (vector) spherical harmonics $\mathcal{Y}^M_{kwu}$ in the equations of Table I are defined as

$$\mathcal{Y}^M_{0wu}(\hat{\mathbf{r}})\equiv(4\pi)^{-1/2}Y_{w,M}(\hat{\mathbf{r}}), \tag{6}$$

$$\mathcal{Y}^M_{1wu}(\hat{\mathbf{r}},\boldsymbol{\sigma})\equiv\sum_m(1-m\,w\,m+M|u\,M)Y_{w,m+M}(\hat{\mathbf{r}})\sqrt{\frac{3}{4\pi}}\sigma_{-m}, \tag{7}$$

where $\boldsymbol{\sigma}$ is the Pauli spin vector, $Y_{w,M}(\hat{\mathbf{r}})$ are the spherical harmonics and $\hat{\mathbf{r}}$ is the unit coordinate vector for the angles in spherical coordinates. The quantity $j_w(qr_s)$ is the spherical Bessel function.

The geometric factors in Eq. (4) are defined as

$$S_{ku}(\kappa)=\begin{cases}\sqrt{2(2j+1)}W\left(\frac{1}{2}\,1\,j\,l\,;\frac{1}{2}\,u\right)\delta_{lw}, & \text{for } k=1\\ \sqrt{\frac{2j+1}{2l+1}}\delta_{lw}, & \text{for } k=0\end{cases} \tag{8}$$

and

$$S'_{ku}(-\kappa)=S_\kappa S_{ku}(-\kappa), \tag{9}$$

where S_κ is the sign of κ. Here $\kappa>0$ corresponds to $l=\kappa$ and $j=l-1/2$ and $\kappa<0$ to $l=-\kappa-1$ and $j=l+1/2$. The angular momenta l and $\bar{l}$ correspond to κ and $-\kappa$, respectively.

The coefficients $g_\mathrm{V}\equiv g_\mathrm{V}(q)$ and $g_\mathrm{A}\equiv g_\mathrm{A}(q)$ in Eq. (4) are the usual weak vector and axial-vector couplings at finite momentum transfer $q>0$. The conserved vector current (CVC) and partially conserved axial-vector current (PCAC) hypotheses give the values $g_\mathrm{V}(0)=1.00$ and $g_\mathrm{A}(0)=1.27$ for a free nucleon at zero momentum transfer, and for finite momentum transfer we can use the dipole approximation [3]. For these couplings deviations from the CVC and PCAC values have been recorded at zero momentum transfer [32,36]). For the induced pseudoscalar coupling g_P the Goldberger-Treiman PCAC relation [37] gives $g_\mathrm{P}/g_\mathrm{A}=7.0$. In this work we choose the slightly quenched values of $g_\mathrm{A}(0)=0.8$ and $g_\mathrm{P}(0)=7.0$ and keep the CVC value $g_\mathrm{V}(0)=1.00$.

The expression (4) can be expanded in powers of the small quantity $1/M^2$. In this way one ends up with the explicit formula $P=P_0+P_1$, where P_0 is the part that one obtains by neglecting all terms of order $1/M^2$ (except for terms containing g_P^2, which is large compared with the other coupling constants) and P_1 contains the rest of the $1/M^2$ terms. For nth forbidden OMC transitions the P_0 term can be written as

$$\begin{aligned}
P_0=&\,g_\mathrm{V}^2[0\,n\,n]^2+\frac{1}{3}g_\mathrm{A}^2([1\,n\,n]^2+[1\,n\,n+1]^2+[1\,n+2\,n+1]^2)+\frac{1}{2n+1}g_\mathrm{V}^2\frac{q}{M}[0\,n\,n](n[0\,n\,n+]+(n+1)[0\,n\,n-])\\
&+\sqrt{\frac{n(n+1)}{3}}\frac{1}{2n+1}g_\mathrm{V}^2\frac{q}{M}(1+\mu_p-\mu_n)[0\,n\,n](-[1\,n\,n-]+[1\,n\,n+])-\sqrt{\frac{n(n+1)}{3}}\frac{1}{2n+1}g_\mathrm{A}g_\mathrm{V}\frac{q}{M}[1\,n\,n]([0\,n\,n-]\\
&-[0\,n\,n+])+\frac{1}{3}g_\mathrm{A}g_\mathrm{V}\frac{q}{M}(1+\mu_p-\mu_n)\Bigg\{\frac{1}{2n+1}[1\,n\,n](n[1\,n\,n-]+(n+1)[1\,n\,n+])\\
&+\frac{1}{2n+3}(\sqrt{n+2}[1\,n\,n+1]-\sqrt{n+1}[1\,n+2\,n+1])(\sqrt{n+2}[1\,n\,n+1-]-\sqrt{n+1}[1\,n+2\,n+1+])\Bigg\}\\
&+\frac{1}{3(2n+3)}g_\mathrm{A}(g_\mathrm{A}-g_\mathrm{P})\frac{q}{M}(\sqrt{n+1}[1\,n\,n+1]+\sqrt{n+2}[1\,n+2\,n+1])(\sqrt{n+1}[1\,n\,n+1-]\\
&+\sqrt{n+2}[1\,n+2\,n+1+])-\frac{2}{\sqrt{3(2n+1)}}g_\mathrm{V}^2\frac{1}{M}[0\,n\,n](\sqrt{n}[1\,n-1\,n\,p]+\sqrt{n+1}[1\,n+1\,n\,p])\\
&-\frac{2}{3}g_\mathrm{A}g_\mathrm{V}\frac{1}{M}\Bigg\{\frac{1}{\sqrt{2n+3}}(-\sqrt{n+2}[1\,n\,n+1]+\sqrt{n+1}[1\,n+2\,n+1])[1\,n+1\,n+1\,p]\\
&+\frac{1}{\sqrt{2n+1}}[1\,n\,n](\sqrt{n+1}[1\,n-1\,n\,p]-\sqrt{n}[1\,n+1\,n\,p])\Bigg\}+\frac{2}{\sqrt{3(2n+3)}}g_\mathrm{A}^2\frac{1}{M}(\sqrt{n+1}[1\,n\,n+1]\\
&+\sqrt{n+2}[1\,n+2\,n+1])[0\,n+1\,n+1\,p]+\frac{1}{12(2n+3)}\left(\frac{g_\mathrm{P}q}{M}\right)^2(\sqrt{n+1}[1\,n\,n+1-]+\sqrt{n+2}[1\,n+2\,n+1+])^2,
\end{aligned} \tag{10}$$

which is the explicit form that can be found in Ref. [33]. Here we use the abbreviation $[k\,w\,u\,(\frac{\pm}{p})]:=\mathcal{M}[k\,w\,u\,(\frac{\pm}{p})]$.

We introduce in our calculations also the next-to-leading-order term P_1 in the expansion $P=P_0+P_1$, which can be derived from Eq. (4). It is needed for OMC transitions, which are quite weak, usually for captures to high-lying states of high

multipolarity, in order to avoid nonphysical negative OMC rates. The term P_1 for nth forbidden transitions reads as

$$
\begin{aligned}
P_1 = &\left(\frac{g_{\rm A}}{M}\right)^2 [0\,n+1\,n+1]^2 + g_{\rm V}^2\left(\frac{q}{2M}\right)^2 \frac{1}{2n+1}(n[0\,n\,n+]^2 + (n+1)[0\,n\,n-]^2) + \frac{1}{3}\left(\frac{g_{\rm V}}{M}\right)^2 ([1\,n-1\,n\,p]^2 \\
&+ [1\,n+1\,n\,p]^2 + [1\,n+1\,n+1\,p]^2) + \frac{1}{12}\left(g_{\rm A}^2 - 2g_{\rm A}g_{\rm P}\right)\left(\frac{q}{M}\right)^2 \frac{1}{2n+3}(\sqrt{n+2}[1\,n+2\,n+1\,+] \\
&+ \sqrt{n+1}[1\,n\,n+1\,-])^2 + \frac{1}{12}\left(\frac{g_{\rm V}q}{2M}\right)^2 (1+\mu_p-\mu_n)\left\{\frac{1}{2n+1}((n+1)[1\,n\,n+]^2\right. \\
&\left. + n[1\,n\,n-]^2) + \frac{1}{2n+3}(\sqrt{n+1}[1\,n+2\,n+1\,+] - \sqrt{n+2}[1\,n\,n+1\,-])^2\right\} \\
&- \frac{1}{\sqrt{3(2n+1)}}\left(\frac{g_{\rm V}}{M}\right)^2 q(\sqrt{n}[1\,n-1\,n\,p][0\,n\,n+] + \sqrt{n+1}[1\,n+1\,n\,p][0\,n\,n-]) \\
&+ \frac{1}{3}\left(\frac{g_{\rm V}}{M}\right)^2 q(1+\mu_p-\mu_n)\left\{\frac{1}{\sqrt{2n+1}}(\sqrt{n}[1\,n+1\,n\,p][1\,n\,n-] - \sqrt{n+1}[1\,n-1\,n\,p][1\,n\,n+])\right. \\
&\left. + \frac{1}{\sqrt{2n+3}}(\sqrt{n+2}[1\,n+1\,n+1\,p][1\,n\,n+1\,-] - \sqrt{n+1}[1\,n+1\,n+1\,p][1\,n+2\,n+1\,+])\right\} \\
&+ \frac{1}{2\sqrt{3}}\left(\frac{g_{\rm V}q}{M}\right)^2 (1+\mu_p-\mu_n)\frac{\sqrt{n(n+1)}}{2n+1}([0\,n\,n+][1\,n\,n+] - [0\,n\,n-][1\,n\,n-]) \\
&+ \frac{1}{\sqrt{3}}g_{\rm A}(g_{\rm A}-g_{\rm P})\frac{q}{M^2}\frac{1}{\sqrt{2n+3}}[0\,n+1\,n+1\,p](\sqrt{n+2}[1\,n+2\,n+1\,+] + \sqrt{n+1}[1\,n\,n+1\,-]). \qquad (11)
\end{aligned}
$$

B. pnQRPA and the Hamiltonian parameters

In this section we introduce the spherical version of the pnQRPA and discuss briefly the determination of the parameter values of its Hamiltonian. The wave functions and excitation energies for the complete set of J^π excitations in the odd-odd daughter nuclei are obtained by performing a pnQRPA diagonalization in the unperturbed basis of quasiproton-quasineutron pairs coupled to J^π. The resulting pnQRPA states in odd-odd nuclei are then of the form

$$
\left|J_k^\pi M\right\rangle = \sum_{pn}\left[X_{pn}^{J_k^\pi} A_{pn}^\dagger(JM) - Y_{pn}^{J_k^\pi}\tilde{A}_{pn}(JM)\right]|\text{pnQRPA}\rangle, \qquad (12)
$$

where k numbers the states of spin-parity J^π, the amplitudes X and Y are the forward- and backward-going pnQRPA amplitudes, $A^\dagger$ and $\tilde{A}$ the quasiproton-quasineutron creation and annihilation operators, M the z projection of J and $|\text{pnQRPA}\rangle$ the pnQRPA vacuum. The transition density corresponding to a transition from a $0_{\rm gs}^+$ initial state to a J_k^π final state can then be written as

$$
\left(J_k^\pi||[c_p^\dagger\tilde{c}_n]_J||0_{\rm gs}^+\right) = \sqrt{2J+1}\left[u_p v_n X_{pn}^{J_k^\pi} + v_p u_n Y_{pn}^{J_k^\pi}\right]. \qquad (13)
$$

The formalism is explained in detail in Refs. [24,38].

The X and Y amplitudes in Eq. (12) are calculated by diagonalizing the pnQRPA matrix separately for each multipole J^π. We follow the partial isospin-restoration scheme introduced in Ref. [39], in which the isoscalar ($T=0$) and isovector ($T=1$) parts of the particle-particle G-matrix elements are multiplied by factors $g_{\rm pp}^{T=0}$ and $g_{\rm pp}^{T=1}$, respectively, for all the multipoles. The isovector parameter $g_{\rm pp}^{T=1}$ is adjusted such that the Fermi part of the corresponding two-neutrino double β ($2\nu\beta\beta$) NME vanishes. The isoscalar parameter $g_{\rm pp}^{T=0}$ is then independently varied to reproduce the $2\nu\beta\beta$-decay half-life. In addition, the particle-hole part was scaled by a common factor $g_{\rm ph}$, fixed by fitting the centroid of the Gamow-Teller giant resonance (GTGR) in the 1^+ channel of the calculations in the usual way. These renormalization factors are adopted from Ref. [31] except for the case $A=82$, which was not included in there. For $A=82$ the corresponding parameter values are $g_{\rm pp}^{T=0}=0.82$, $g_{\rm pp}^{T=1}=0.95$, and $g_{\rm ph}=0.997$.

We adopt for each even-even nucleus involved in the computations the single-particle bases used in the isovector spin-multipole calculations of Refs. [28,31], i.e., no-core bases with all the orbitals from the $N=0$ oscillator major shell up to at least two oscillator major shells above the respective Fermi surfaces for both protons and neutrons. The single-particle energies were obtained by solving the radial Schrödinger equation for a Coulomb-corrected Woods-Saxon (WS) potential, optimized for nuclei close to the β-stability line [40]. This choice is justified since the $\beta\beta$-decaying nuclei lie always rather close to the bottom of the valley of β stability. Both the bound and quasibound single-particle states are active in the calculations. The single-particle energies close to the proton and neutron Fermi surfaces were slightly modified in order to better reproduce the low-lying spectra of the neighboring odd-mass nuclei at the BCS quasiparticle level.

The quasiparticle spectra for protons and neutrons, needed in the pnQRPA diagonalization, are obtained by solving the BCS equations for protons and neutrons, separately. In our calculations the two-body interaction is derived from the Bonn-A one-boson-exchange potential introduced in Ref. [41]. The calculated BCS pairing gaps are fitted (see

TABLE II. pnQRPA-computed and Primakoff-formula based total rates for OMC on different parent nuclei (Parent), as well as the effective Z values. Axial couplings $g_A(0) = 0.8$ and $g_P(0) = 7.0$ were adopted in the calculations.

Parent	Z_{eff}	$W_{\text{pnQRPA}}(10^6/\text{s})$	$W_{\text{Pr.}}(10^6/\text{s})$
^{76}Se	24.47 (for $Z = 37$)	16.4	8.3
^{82}Kr	24.47 (for $Z = 37$)	16.5	7.5
^{96}Mo	26.37	20.4	10.0
^{100}Ru	26.37 (for $Z = 42$)	16.7	10.3
^{116}Sn	28.64	15.7	12.7
^{128}Xe	29.99 (for $Z = 56$)	21.2	13.3
^{130}Xe	29.99 (for $Z = 56$)	23.6	11.9
^{136}Ba	29.99	21.1	11.1

Refs. [24,38,42,43]) to the phenomenological proton and neutron pairing gaps in a way described in detail in Ref. [28]. The values of the resulting pairing scaling factors are listed in Refs. [28,31].

III. RESULTS AND DISCUSSION

In this section we present and discuss the results of our studies. The style of presentation of the results serves the purpose of easy comparison with future experimental data.

A. OMC strength functions in intermediate nuclei of $0\nu\beta\beta$ decays

An approximation for the total OMC rate on nucleus $^A_Z X$ can be computed using the Primakoff formula [34]

$$W_{\text{Pr.}}(A, Z) = Z_{\text{eff}}^4 X_1 \left[1 - X_2\left(\frac{A - Z}{2A}\right)\right], \qquad (14)$$

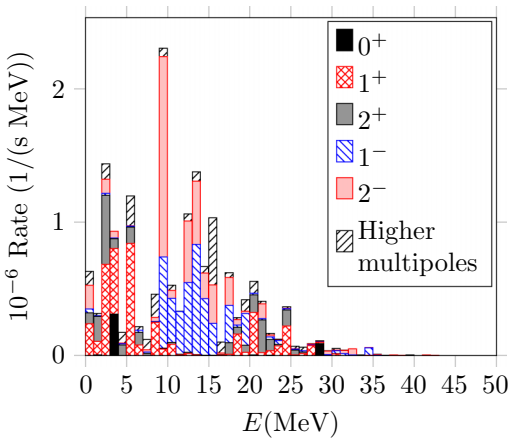

FIG. 1. OMC on ^{76}Se: muon-capture-rate distribution (OMC strength function) in ^{76}As. Transition strengths to $J^\pi_f = 0^+, 1^\pm, 2^\pm$ states and to states of higher multipolarity are separated. The y axis gives the capture rate in millions of captures per second and per MeV. The horizontal axis shows the excitation energy in the ^{76}As nucleus. Here a 1.0 MeV binning in energy is used and coupling strengths $g_A(0) = 0.8$ and $g_P(0) = 7.0$ were adopted in the calculations.

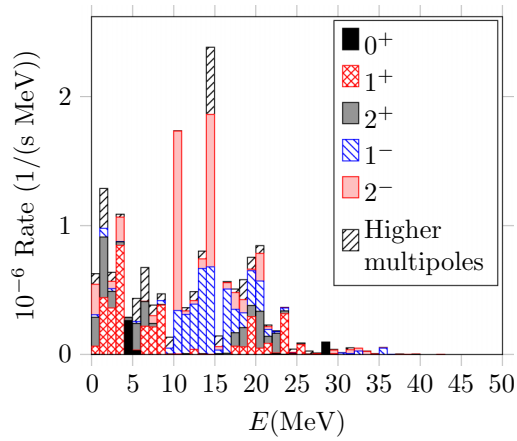

FIG. 2. The same as in Fig. 1 but for captures on ^{82}Kr to states in ^{82}Br.

where A, Z, and Z_{eff} are the mass number, atomic number, and effective atomic number of the nucleus, X_1 the reduced muon-capture rate for OMC on hydrogen, and X_2 a parameter that takes into account the Pauli exclusion principle. We adopt the typical values

$$X_1 = 170\ 1/\text{s} \quad \text{and} \quad X_2 = 3.125.$$

for the X factors.

In Table II we list for each nucleus of interest the effective Z values Z_{eff} obtained from the work of Ford and Wills [35], and the total muon capture rates obtained from the Primakoff formula (14) as well as the total capture rate of Eq. (2) obtained from the pnQRPA calculations. The pnQRPA results include transition rates to all possible multipole states summed over an energy region of 0–55 MeV. The moderately quenched parameter values $g_A(0) = 0.8$ and $g_P(0) = 7.0$ were adopted in the calculations.

We notice that using the parameter values $g_A(0) = 0.8$ and $g_P(0) = 7.0$ the pnQRPA formalism gives larger capture rates than the corresponding Primakoff estimates. However, it was noticed in Ref. [29] that decreasing the value of g_A or increasing the value of g_P decreases the total capture rate. In terms of

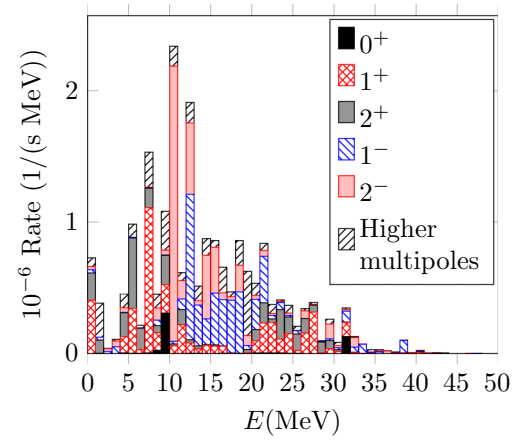

FIG. 3. The same as in Fig. 1 but for captures on ^{96}Mo to states in ^{96}Nb.

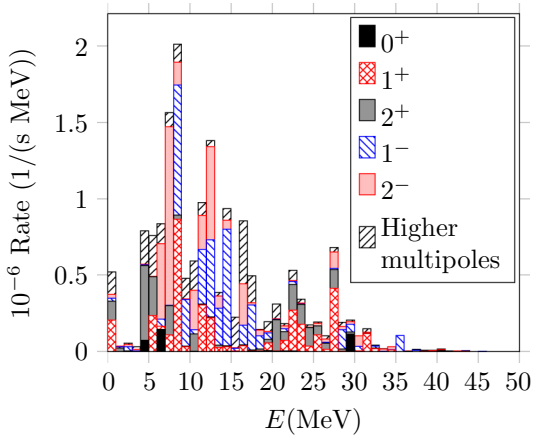

FIG. 4. The same as in Fig. 1 but for captures on ^{100}Ru to states in ^{100}Tc.

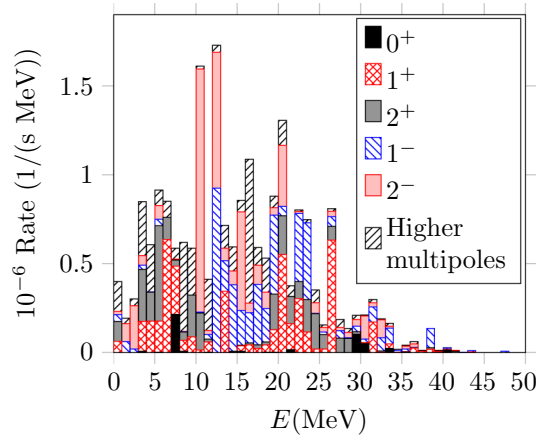

FIG. 6. The same as in Fig. 1 but for captures on ^{128}Xe to states in ^{128}I.

the axial coupling, the Primakoff rates can be reproduced by a strongly quenched effective value of $g_A(0) \approx 0.5$.

In Figs. 1–8 we present the OMC strength functions for the captures on ^{76}Se, ^{82}Kr, ^{96}Mo, ^{100}Ru, ^{116}Sn, ^{128}Xe, ^{130}Xe, and ^{136}Ba obtained from Eq. (2) with the parameter values $g_A(0) = 0.8$ and $g_P(0) = 7.0$. We separately indicate the OMC rates to $J^\pi = 0^+, 1^\pm, 2^\pm$ states of the daughter nuclei (the intermediate nuclei of $0\nu\beta\beta$ decays) and also give the total capture rate, which includes transitions to states of all possible multipolarities. The results are presented using a 1.0 MeV binning in energy. One can see that transitions to $J^\pi = 0^+, 1^\pm, 2^\pm$ states form the majority of the total capture rates, transitions to states of higher multipolarity forming only some 10–20% of the total capture rate.

In Tables VI–XIII (see the Appendix) we present the relative capture rates $W(J^\pi)/W_{\text{tot}}$ (%) to states of different multipolarities corresponding to Figs. 1–8. Here the numbers of the bins refer to the different energy bins in the figures: Bin No. 1 refers to the 0–1 MeV energy bin and so on. These tables are handy when one wants to compare the OMC distributions obtained in future muon experiments with the presently calculated ones.

In Ref. [29] the first theoretical evidence of an OMC giant resonance was produced for the OMC on ^{100}Mo. In that work it was seen that the computed location of the resonance agreed well with the experimentally determined one. Also from Figs. 1–8 one can observe structures of the OMC strength functions, which would correspond to an OMC giant resonance. In Figs. 1 (OMC on ^{76}Se) and 3 (OMC on ^{96}Mo) the centroid of a resonancelike structure can be observed at around 12 MeV, in Fig. 2 (OMC on ^{82}Kr) the resonance is around 14 MeV, in Fig. 4 (OMC on ^{100}Ru) the resonance is around 10 MeV, and in Fig. 6 (OMC on ^{128}Xe) a broad resonancelike structure is found around 14 MeV. For the OMC on the heaviest two nuclei, ^{130}Xe and ^{136}Ba, no clear resonance can be identified, but rather a wide flat region of strong captures to states below about 18 MeV. Also for the OMC on ^{116}Sn, Fig. 5, no clear giant resonance can be identified.

The resonancelike structures are dominated by the $1\hbar\omega$ excitations of multipolarities $J^\pi = 1^-, 2^-$. For the OMC on ^{76}Se and ^{82}Kr there is a visible low-energy satellite of the OMC resonance consisting mainly of $0\hbar\omega$ excitations of multipolarities $J^\pi = 1^+, 2^+$. In general, these excitations

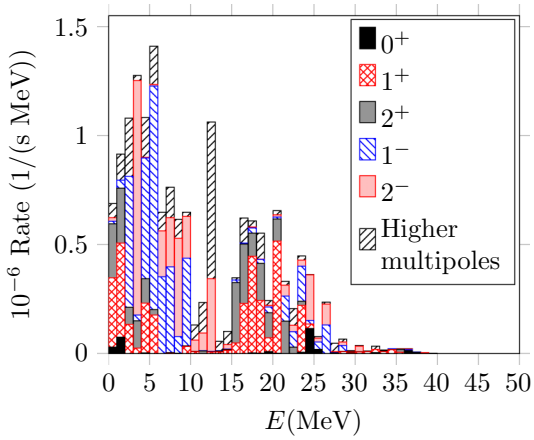

FIG. 5. The same as in Fig. 1 but for captures on ^{116}Sn to states in ^{116}In.

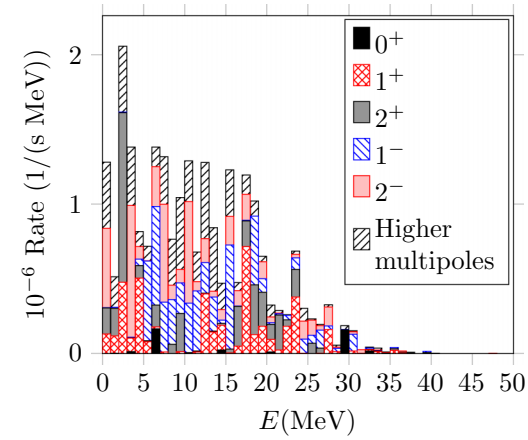

FIG. 7. The same as in Fig. 1 but for captures on ^{130}Xe to states in ^{130}I.

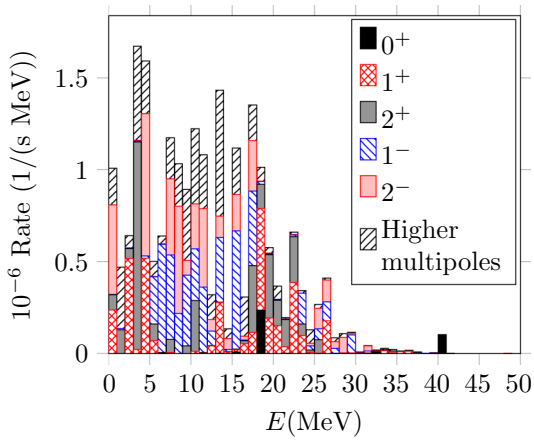

FIG. 8. The same as in Fig. 1 but for captures on ^{136}Ba to states in ^{136}Cs.

play a major role at low energies for all cases. At high energies, 15–28 MeV, the $2\hbar\omega$ excitations of multipolarities $J^\pi = 1^+, 2^+$ dominate forming even a high-energy satellite resonance in the cases of OMC on ^{100}Ru, ^{116}Sn, and ^{128}Xe. At energies of about 28–32 MeV one can see traces of $2\hbar\omega$ $J^\pi = 0^+$ excitations. For the heaviest nuclei these 0^+ contributions can reach up to 40 MeV of excitation. The high-energy tail of the $J^\pi = 1^-, 2^-$ excitations, beyond 24–28 MeV, stems from $3\hbar\omega$ excitations.

B. OMC rates in ^{76}As compared with available data

There is a possibility to compare our pnQRPA-computed rates with data for the OMC on ^{76}Se. In Ref. [2] the OMC rates to states of low excitation in ^{76}As were measured. In the present calculations we use the coupling strengths $g_A(0) = 0.8$ and $g_P(0) = 7.0$.

The experimental OMC rates to different low-energy states of ^{76}As, deduced from the results of Ref. [2], are presented in Table III. The table has been divided in two, and the excitation energies of the states are listed in the first columns, the J^π assignments in the second columns and the capture rates in the third columns. The corresponding pnQRPA results are presented in Table IV.

Let us first compare Tables III and IV. Direct comparison of the tables is hampered by the unknown spin-parities in the experimental energy spectrum. Overall, similar spin-parity assignments J^π and OMC rates of the same order of magnitude are recorded by comparing the numbers of the tables. However, there are much fewer states in the low-energy spectrum computed with the pnQRPA. This is a typical feature of the pnQRPA calculations: The pnQRPA calculations predict less states in odd-odd nuclei than is detected experimentally. However, the corresponding transition strength (in this case OMC rates) is there, but concentrated in few strong states. Usually the centroid of the experimental strength is well reproduced but the fine structure is not due to the too small a configuration space of the pnQRPA approach. In many cases, in low momentum-exchange processes, the pnQRPA strength is concentrated in the lowest collective states, usually of the multipolarities $J^\pi = 1^+, 2^-$ (Gamow-Teller and spin-dipole strength). For high momentum-exchange processes, such as the $0\nu\beta\beta$ decay and the OMC, the strength is gathered by the lowest states with multipolarities $J^\pi = 1^+, 2^\pm, 3^\pm$. The realistic nature of the summed OMC strength of pnQRPA is visible in the obtained total capture rate 6.7×10^5 1/s below 1.1 MeV, which is quite close to the corresponding

TABLE III. OMC on ^{76}Se: measured OMC rates (column 3) to low-energy states of ^{76}As as deduced from Ref. [2]. The table has been cut in two and appears as left and right halves. The excitation energies are displayed in columns 1 and the J^π values in column 2. The OMC rate to the ground state of ^{76}As cannot be measured.

E (MeV)	J^π	Rate (1/s)	E (MeV)	J^π	Rate (1/s)
0.0000	2^-	g.s.	0.6401	$(1^-, 2^-)$	11 520
0.1203	1^+	20 480	0.6691	$(1^+, 2^+)$	40 960
0.1222	$(1)^-$	13 440	0.6811	$(1^-,4)$	21 120
0.165	$(3)^-$	34 560	0.7344	$(\leqslant 4)^-$	5 120
0.2035	$(0,1)^+$	5 120	0.7518	$(0^-,1,2)$	23 680
0.2803	$(1,2)^+$	7 040	0.7566	$(0^+, 3^+)$	16 640
0.2926	$(2,3,4)^-$	3 200	0.7744	$(1^+, 3^+)$	14 720
0.3285	$(3,4)^-$	5 760	0.7936	$(1,2,3)^+$	12 800
0.3524	$(3)^-$	3 200	0.8024	$(1^-, 2^-, 3^+)$	10 880
0.4018	$(1,2)^+$	26 240	0.8633	1^+	17 280
0.4368	$(1,2,3)^-$	17 920	0.8932	$(1^-, 2^-, 3^+)$	14 720
0.4472	$(1,2)^+$	29 440	0.9247	$(\leqslant 3)^-$	15 360
0.471	$(2)^-$	3 200	0.9397	(1,2,3)	21 120
0.4996	$(1^+, 2^-)$	63 360	0.9584	$\leqslant 3$	8 320
0.5052	$(2,3)^+$	16 000	0.9855	$(1,2,3)^+$	13 440
0.5176	$(1,2^+)$	15 360	1.0262	$(1^+, 3^+)$	61 440
0.544	$(2,3)^-$	24 960	1.0342	$(1,2,3)^+$	8 320
0.61	$(1,2,3^-)$	43 520	1.0645	1^+	14 720
				Tot.	664 960

TABLE IV. OMC on ^{76}Se: pnQRPA-computed OMC rates (column 3) to low-energy states of ^{76}As. Coupling strengths $g_A(0) = 0.8$ and $g_P(0) = 7.0$ were adopted in the calculations.

E (MeV)	J^π	Rate (1/s)
0.0	2^-	177 802
0.044	1^+	236 595
0.122	1^-	28 991
0.165	3^-	23 568
0.204	0^+	414.27
0.211	4^-	19 911
0.265	2^+	83 516
0.505	3^+	55 355
0.854	3^-	9 647
1.0	4^+	2 797
1.004	2^+	30 500
1.007	4^-	3 986
1.075	3^-	1 621
	Tot.	670 716

experimental value 6.6×10^5 1/s despite the differences in the rates to the individual states.

The uncertain spin-parity assignments of Table III allow for speculations about the division of the OMC strength between different multipole states. In fact, one can play with the spin-parity assignments of Table III within the limits allowed by the uncertainties. In this way one could try to produce an educated guess of the most probable spin-parity assignments and then sum up the OMC strength multipole by multipole. In this way one creates a kind of most probable experimental OMC strength distribution below about 1.1 MeV. This probable distribution can then be compared with the multipole-by-multipole-summed OMC strength of Table IV for pnQRPA. These two distributions have been gathered into Table V. From the table one immediately sees that the correspondence between the experimental and pnQRPA-computed OMC strength distributions is strikingly good. Only the pnQRPA-computed rate to the 0^+ states is an order of magnitude smaller than the corresponding experimental rate. The deviation might be due to the small deformation of ^{76}Se [44]. It has to be borne in mind that the OMC strength to the 2^- ground state has not been measured since the corresponding γ rays could not be extracted. This experimental deficit in OMC has been indicated by + g.s. in the corresponding row of Table V. Future spin-assignment sensitive measurements will shed light on the reliability of the presently introduced most probable experimental OMC strength distribution.

TABLE V. Comparison of the most probable experimental multipole-by-multipole OMC strength distribution obtained from Table III with the corresponding pnQRPA-computed distribution deduced from Table IV. The OMC strength to the 2^- ground state has not been measured and this is indicated by + g.s. in the corresponding row.

J^π	OMC rate (1/s)	
	Expt.	pnQRPA
0^+	5120	414
1^+	218 240	236 595
1^-	31 360	28 991
2^+	120 960	114 016
2^-	145 920 + g.s.	177 802
3^+	60 160	55 355
3^-	53 120	34 836
4^+	–	2797
4^-	30 080	23 897

IV. CONCLUSIONS

In this work we have calculated the rates of ordinary muon capture on the 0^+ ground states of the daughter nuclei of eight $0\nu\beta\beta$-decaying parent nuclei in the Morita-Fujii formalism of the OMC. The calculations have been performed using the proton-neutron quasiparticle RPA with realistic two-body interactions and slightly modified no-core Woods-Saxon bases. The computed OMC strength functions are presented for the OMC on ^{76}Se, ^{82}Kr, ^{96}Mo, ^{100}Ru, ^{116}Sn, ^{128}Xe, ^{130}Xe, and ^{136}Ba. The computed total OMC capture rates are compared with the corresponding Primakoff estimates. The computed total rates are somewhat larger than the Primakoff values, which suggests a rather strongly quenched effective value of $g_A(0) \approx 0.5$.

The pnQRPA-computed rates of OMC on ^{76}Se to the states below 1.1 MeV in ^{76}As were compared with the available data of Ref. [2]. It was found that the correspondence of the experimental and pnQRPA-computed strength, decomposed in multipoles, is quite good. This, in turn, points to reliability of the present calculations of the OMC strength functions.

Further measurements and computations of the OMC strength functions for final nuclei of double β decays could enable a systematic study of the sensitivity of the OMC strength function to the effective values of the weak axial couplings. This could help improve the accuracy of calculations of the nuclear matrix elements of the neutrinoless double β decay. On the other hand, the OMC provides a promising opportunity for studying the (anti)neutrino responses for medium-energy astroneutrino interactions. Further experimental studies are in progress at RCNP Osaka for nuclei of interest in studies of nuclear double β decay and astroneutrino interactions.

APPENDIX: TABLES FOR RELATIVE OMC RATES

Our pnQRPA-computed relative OMC rates for $g_A(0) = 0.8$ and $g_P(0) = 7.0$ are summarized in Tables VI–XIII. Here the quantities $W(J^\pi)/W_{\text{tot}}$ are given in per cents for multipoles $J^\pi = 0^+, 1^\pm, 2^\pm$ separately, and the rest as a lump sum. The energy bins are numbered such that bin No. n corresponds to the energy interval $[n-1, n]$ MeV. These tables enable easy comparison with the strength functions extracted from future OMC experiments.

TABLE VI. Relative pnQRPA-computed rates to states in ^{76}As for the OMC on ^{76}Se. The rates are given in 1 MeV energy bins as percents of the total OMC rate. There are three separate tables side by side listing the bin numbers (columns 1) and the different multipolarities (columns 2–7). The values $g_A(0) = 0.8$ and $g_P(0) = 7.0$ for the weak couplings were adopted in the calculations.

Bin No.	$W(J^\pi)/W_{tot}(\%)$						Bin No.	$W(J^\pi)/W_{tot}(\%)$						Bin No.	$W(J^\pi)/W_{tot}(\%)$					
	0^+	1^+	2^+	1^-	2^-	Others		0^+	1^+	2^+	1^-	2^-	Others		0^+	1^+	2^+	1^-	2^-	Others
1	0.00	1.44	0.51	0.18	1.08	0.63	16	0.00	0.00	0.01	1.45	1.77	3.05	31	0.00	0.08	0.00	0.14	0.02	0.08
2	0.03	0.61	1.15	0.03	0.00	0.10	17	0.00	0.03	0.01	0.00	0.07	0.51	32	0.00	0.00	0.00	0.08	0.15	0.01
3	0.00	4.17	3.14	0.10	0.65	0.69	18	0.00	0.05	0.53	1.70	1.28	0.22	33	0.00	0.00	0.00	0.02	0.28	0.00
4	1.89	2.99	0.45	0.04	0.30	0.01	19	0.00	0.98	0.31	0.10	0.26	0.08	34	0.00	0.00	0.00	0.00	0.00	0.03
5	0.00	0.00	0.49	0.06	0.03	0.49	20	0.00	0.15	0.31	1.45	0.10	0.53	35	0.00	0.01	0.00	0.34	0.01	0.00
6	0.00	5.11	0.75	0.04	0.01	1.37	21	0.03	1.93	0.81	0.07	0.01	0.53	36	0.00	0.00	0.00	0.01	0.03	0.02
7	0.00	0.49	0.57	0.09	0.00	0.16	22	0.00	0.13	1.50	0.06	0.66	0.12	37	0.00	0.00	0.00	0.00	0.00	0.01
8	0.00	0.00	0.10	0.07	0.10	0.47	23	0.02	0.20	0.52	0.11	0.10	0.06	38	0.00	0.01	0.00	0.00	0.01	0.00
9	0.00	1.50	0.01	0.04	0.19	1.06	24	0.00	0.44	0.07	0.18	0.01	0.05	39	0.00	0.01	0.00	0.00	0.00	0.00
10	0.00	0.29	0.04	4.17	9.16	0.37	25	0.00	1.34	0.74	0.05	0.02	0.07	40	0.01	0.00	0.01	0.00	0.00	0.00
11	0.00	0.51	0.09	2.01	0.36	0.24	26	0.00	0.02	0.23	0.03	0.02	0.12	41	0.00	0.00	0.00	0.00	0.00	0.00
12	0.00	0.02	0.04	1.94	0.01	0.00	27	0.00	0.09	0.06	0.06	0.00	0.16	42	0.00	0.02	0.00	0.00	0.00	0.00
13	0.00	0.08	0.06	3.18	2.82	0.31	28	0.00	0.44	0.01	0.02	0.05	0.02	43	0.00	0.01	0.00	0.00	0.00	0.00
14	0.00	0.02	0.03	5.02	2.89	0.43	29	0.54	0.07	0.00	0.00	0.01	0.05							
15	0.00	0.00	0.01	2.59	1.17	0.29	30	0.00	0.00	0.00	0.03	0.16	0.01							

TABLE VII. The same as in Table VI but for OMC on ^{82}Kr to states in ^{82}Br.

Bin No.	$W(J^\pi)/W_{tot}(\%)$						Bin No.	$W(J^\pi)/W_{tot}(\%)$						Bin No.	$W(J^\pi)/W_{tot}(\%)$					
	0^+	1^+	2^+	1^-	2^-	Others		0^+	1^+	2^+	1^-	2^-	Others		0^+	1^+	2^+	1^-	2^-	Others
1	0.01	0.38	1.36	0.12	1.43	0.50	16	0.00	0.00	0.05	0.17	0.16	0.49	31	0.00	0.00	0.00	0.07	0.01	0.01
2	0.00	2.67	2.85	0.40	0.00	1.87	17	0.00	0.00	0.05	3.02	0.30	0.05	32	0.00	0.00	0.00	0.04	0.18	0.09
3	0.00	2.19	0.78	0.12	0.35	0.42	18	0.00	0.39	0.63	1.10	0.78	0.17	33	0.00	0.00	0.00	0.16	0.14	0.00
4	0.00	5.13	0.17	0.01	1.16	0.13	19	0.00	0.37	0.89	0.70	0.61	0.94	34	0.00	0.00	0.00	0.00	0.14	0.03
5	1.60	0.00	0.13	0.00	0.01	0.01	20	0.00	1.78	0.53	1.62	0.09	0.55	35	0.00	0.00	0.00	0.00	0.03	0.01
6	0.19	0.02	1.26	0.08	0.00	1.09	21	0.00	0.29	1.75	1.41	1.31	0.35	36	0.00	0.00	0.00	0.30	0.02	0.01
7	0.00	1.32	1.17	0.00	0.02	1.58	22	0.01	0.52	0.34	0.31	0.15	0.07	37	0.00	0.00	0.00	0.01	0.00	0.00
8	0.00	1.29	0.17	0.00	0.37	0.49	23	0.04	0.04	0.91	0.08	0.00	0.04	38	0.00	0.01	0.02	0.00	0.00	0.00
9	0.00	2.32	0.03	0.18	0.00	0.31	24	0.02	1.91	0.13	0.13	0.01	0.02	39	0.00	0.01	0.00	0.00	0.00	0.00
10	0.00	0.01	0.01	0.28	0.00	0.52	25	0.00	0.01	0.04	0.01	0.05	0.14	40	0.01	0.01	0.00	0.00	0.00	0.00
11	0.00	0.03	0.00	2.04	8.45	0.01	26	0.00	0.46	0.06	0.00	0.00	0.01	41	0.00	0.00	0.00	0.00	0.00	0.00
12	0.00	0.00	0.04	1.85	0.17	0.15	27	0.00	0.02	0.01	0.00	0.00	0.14	42	0.00	0.00	0.00	0.00	0.00	0.00
13	0.00	0.24	0.00	2.13	0.16	0.43	28	0.00	0.04	0.00	0.00	0.00	0.02	43	0.00	0.01	0.00	0.00	0.00	0.00
14	0.00	0.01	0.02	4.01	0.45	0.36	29	0.51	0.00	0.02	0.01	0.00	0.05							
15	0.00	0.01	0.00	4.11	7.18	3.15	30	0.00	0.04	0.00	0.01	0.17	0.03							

TABLE VIII. The same as in Table VI but for OMC on ^{96}Mo to states in ^{96}Nb.

Bin No.	$W(J^\pi)/W_{\rm tot}(\%)$						Bin No.	$W(J^\pi)/W_{\rm tot}(\%)$						Bin No.	$W(J^\pi)/W_{\rm tot}(\%)$					
	0^+	1^+	2^+	1^-	2^-	Others		0^+	1^+	2^+	1^-	2^-	Others		0^+	1^+	2^+	1^-	2^-	Others
1	0.00	1.99	1.02	0.12	0.12	0.33	17	0.01	0.27	0.01	1.72	0.25	0.96	33	0.00	0.04	0.00	0.19	0.36	0.04
2	0.01	0.00	0.49	0.11	0.00	1.27	18	0.00	0.01	0.01	1.97	0.13	0.17	34	0.00	0.01	0.00	0.33	0.01	0.00
3	0.00	0.00	0.00	0.08	0.10	0.02	19	0.00	0.00	0.01	2.29	1.00	0.92	35	0.00	0.01	0.00	0.03	0.01	0.09
4	0.00	0.00	0.00	0.25	0.22	0.06	20	0.00	0.03	0.13	0.14	0.38	2.39	36	0.00	0.00	0.00	0.05	0.04	0.05
5	0.02	0.62	0.89	0.01	0.17	0.51	21	0.03	0.45	0.42	1.12	0.15	0.45	37	0.00	0.00	0.00	0.00	0.10	0.00
6	0.01	1.67	2.62	0.03	0.00	0.49	22	0.02	1.12	0.76	1.73	0.22	0.26	38	0.00	0.02	0.01	0.01	0.00	0.02
7	0.01	0.14	0.81	0.00	0.01	0.10	23	0.02	1.14	0.13	0.13	0.07	0.34	39	0.00	0.01	0.01	0.47	0.00	0.02
8	0.03	5.41	0.73	0.00	0.03	1.30	24	0.02	0.52	1.10	0.26	0.04	0.06	40	0.00	0.02	0.01	0.00	0.00	0.00
9	0.12	0.66	0.26	0.21	0.45	0.51	25	0.01	0.74	0.61	0.06	0.09	0.29	41	0.00	0.05	0.03	0.03	0.00	0.00
10	1.50	1.07	1.09	0.00	0.18	1.45	26	0.02	0.09	0.62	0.12	0.01	0.16	42	0.00	0.01	0.01	0.00	0.00	0.00
11	0.00	0.28	0.08	0.09	10.27	0.74	27	0.00	0.77	0.54	0.01	0.28	0.08	43	0.03	0.00	0.00	0.00	0.00	0.00
12	0.00	1.08	0.56	0.39	0.68	0.30	28	0.00	1.55	0.26	0.01	0.02	0.07	44	0.00	0.00	0.02	0.00	0.00	0.00
13	0.01	0.38	0.12	5.44	2.66	0.77	29	0.00	0.02	0.41	0.02	0.00	0.02	45	0.00	0.00	0.00	0.00	0.00	0.00
14	0.00	0.17	0.12	1.52	0.17	0.54	30	0.00	0.18	0.31	0.06	0.55	0.18	46	0.00	0.00	0.00	0.00	0.00	0.00
15	0.00	0.32	0.01	0.97	2.36	0.63	31	0.00	0.07	0.07	0.06	0.09	0.12	47	0.00	0.00	0.00	0.00	0.00	0.00
16	0.00	0.27	0.05	1.93	1.71	0.25	32	0.63	0.53	0.01	0.40	0.06	0.07	48	0.00	0.00	0.00	0.01	0.00	0.00

TABLE IX. The same as in Table VI but for OMC on ^{100}Ru to states in ^{100}Tc.

Bin No.	$W(J^\pi)/W_{\rm tot}(\%)$						Bin No.	$W(J^\pi)/W_{\rm tot}(\%)$						Bin No.	$W(J^\pi)/W_{\rm tot}(\%)$					
	0^+	1^+	2^+	1^-	2^-	Others		0^+	1^+	2^+	1^-	2^-	Others		0^+	1^+	2^+	1^-	2^-	Others
1	0.00	1.23	0.73	0.11	0.16	0.88	16	0.00	0.02	0.00	0.11	0.03	1.19	31	0.00	0.02	0.01	0.18	0.41	0.01
2	0.00	0.00	0.13	0.05	0.02	0.00	17	0.00	0.23	0.03	0.78	1.62	2.47	32	0.00	0.71	0.00	0.00	0.04	0.13
3	0.03	0.00	0.00	0.16	0.09	0.05	18	0.01	0.02	0.03	1.77	0.08	1.07	33	0.00	0.12	0.01	0.08	0.00	0.03
4	0.00	0.00	0.00	0.02	0.06	0.10	19	0.01	0.01	0.08	0.51	0.23	0.03	34	0.00	0.00	0.00	0.00	0.09	0.01
5	0.44	0.00	2.93	0.02	0.02	1.31	20	0.03	0.31	0.13	0.25	0.06	0.39	35	0.00	0.07	0.00	0.00	0.12	0.00
6	0.00	1.40	1.53	0.00	0.01	1.60	21	0.01	0.02	1.22	0.01	0.03	0.57	36	0.00	0.00	0.00	0.62	0.00	0.01
7	0.87	0.13	0.00	0.28	2.95	0.79	22	0.03	0.41	0.34	0.11	0.11	0.09	37	0.01	0.00	0.00	0.01	0.00	0.00
8	0.00	0.65	1.15	0.01	6.99	0.56	23	0.02	1.60	1.01	0.12	0.04	0.40	38	0.00	0.00	0.00	0.05	0.00	0.04
9	0.00	5.19	0.16	5.10	0.89	0.70	24	0.00	1.07	0.79	0.00	0.05	0.14	39	0.00	0.02	0.02	0.00	0.00	0.02
10	0.00	0.19	0.02	1.83	0.02	0.81	25	0.00	0.21	0.73	0.01	0.01	0.08	40	0.00	0.04	0.00	0.00	0.00	0.00
11	0.01	0.00	0.68	0.16	1.55	1.14	26	0.00	0.65	0.35	0.00	0.10	0.05	41	0.03	0.04	0.03	0.00	0.00	0.00
12	0.00	1.83	0.03	2.14	1.34	0.51	27	0.00	0.08	0.24	0.04	0.13	0.13	42	0.00	0.00	0.02	0.00	0.00	0.00
13	0.00	1.32	0.04	3.03	3.64	0.24	28	0.00	2.48	0.73	0.05	0.64	0.17	43	0.00	0.02	0.00	0.00	0.00	0.00
14	0.00	0.16	0.10	1.44	0.48	0.14	29	0.00	0.02	0.08	0.75	0.13	0.16	44	0.00	0.01	0.02	0.01	0.00	0.00
15	0.00	0.18	0.05	4.56	0.35	0.46	30	0.68	0.01	0.09	0.30	0.10	0.06							

TABLE X. The same as in Table VI but for OMC on ^{116}Sn to states in ^{116}In.

Bin No.	$W(J^\pi)/W_{\rm tot}(\%)$						Bin No.	$W(J^\pi)/W_{\rm tot}(\%)$						Bin No.	$W(J^\pi)/W_{\rm tot}(\%)$					
	0^+	1^+	2^+	1^-	2^-	Others		0^+	1^+	2^+	1^-	2^-	Others		0^+	1^+	2^+	1^-	2^-	Others
1	0.00	2.12	0.95	0.08	0.14	0.41	14	0.00	0.05	0.04	0.00	0.00	0.27	27	0.01	0.00	0.00	0.85	0.61	0.06
2	0.21	2.70	2.39	0.23	0.00	0.76	15	0.01	0.09	0.07	0.01	0.14	0.38	28	0.01	0.00	0.01	0.00	0.04	0.24
3	0.35	0.89	0.37	4.03	0.00	1.71	16	0.00	0.02	1.76	0.09	0.00	0.06	29	0.00	0.03	0.01	0.17	0.11	0.09
4	0.00	0.09	0.72	0.12	6.86	0.15	17	0.00	1.64	1.74	0.01	0.00	0.73	30	0.01	0.03	0.02	0.00	0.02	0.03
5	0.03	1.51	0.81	3.51	0.01	1.17	18	0.01	2.89	0.60	0.19	0.04	0.18	31	0.01	0.05	0.00	0.01	0.16	0.02
6	0.14	1.12	0.12	5.96	0.03	1.11	19	0.04	1.56	1.13	0.06	0.00	0.76	32	0.00	0.06	0.00	0.00	0.00	0.01
7	0.00	0.00	0.00	2.10	1.36	0.55	20	0.03	0.40	0.74	0.16	0.04	0.15	33	0.03	0.09	0.00	0.01	0.00	0.09
8	0.00	0.01	0.01	1.51	1.43	0.90	21	0.00	3.29	0.59	0.07	0.07	0.12	34	0.00	0.06	0.02	0.00	0.00	0.02
9	0.00	0.00	0.00	1.59	2.92	0.56	22	0.00	0.00	1.02	0.73	0.39	0.11	35	0.00	0.11	0.06	0.02	0.00	0.00
10	0.00	0.21	0.00	2.71	1.29	0.13	23	0.00	0.00	0.19	0.45	0.13	0.49	36	0.00	0.04	0.02	0.00	0.01	0.00
11	0.00	0.06	0.03	0.00	0.27	0.44	24	0.01	1.37	0.12	1.01	0.99	0.12	37	0.05	0.00	0.03	0.03	0.02	0.00
12	0.00	0.00	0.07	0.01	1.78	0.89	25	0.71	0.14	0.00	0.10	0.54	0.01	38	0.00	0.00	0.03	0.01	0.00	0.00
13	0.01	0.04	0.01	0.01	0.83	4.59	26	0.18	0.00	0.00	0.19	0.11	0.04	39	0.00	0.02	0.00	0.00	0.00	0.00

TABLE XI. The same as in Table VI but for OMC on ^{128}Xe to states in ^{128}I.

Bin No.	$W(J^\pi)/W_{\rm tot}(\%)$						Bin No.	$W(J^\pi)/W_{\rm tot}(\%)$						Bin No.	$W(J^\pi)/W_{\rm tot}(\%)$					
	0^+	1^+	2^+	1^-	2^-	Others		0^+	1^+	2^+	1^-	2^-	Others		0^+	1^+	2^+	1^-	2^-	Others
1	0.00	0.29	0.53	0.18	0.09	0.80	17	0.00	0.20	0.05	0.80	0.26	3.82	33	0.00	0.00	0.04	0.35	0.48	0.03
2	0.00	0.00	0.00	0.29	0.48	0.15	18	0.00	0.11	0.10	1.60	0.52	0.46	34	0.11	0.12	0.00	0.42	0.06	0.08
3	0.00	0.00	0.00	0.09	1.15	0.18	19	0.00	0.20	0.07	0.89	0.43	0.91	35	0.00	0.01	0.00	0.04	0.00	0.03
4	0.03	0.79	1.38	0.11	0.25	1.44	20	0.01	0.59	0.95	2.09	0.20	0.30	36	0.02	0.01	0.00	0.07	0.08	0.03
5	0.00	0.83	0.77	0.01	0.00	1.25	21	0.00	2.60	1.03	0.25	1.62	0.66	37	0.00	0.12	0.01	0.00	0.09	0.06
6	0.01	0.83	2.53	0.17	0.37	0.41	22	0.07	0.70	0.72	0.00	0.00	0.28	38	0.00	0.03	0.02	0.00	0.00	0.01
7	0.00	3.00	0.58	0.00	0.00	0.42	23	0.00	1.43	0.45	1.81	0.05	0.05	39	0.00	0.08	0.04	0.52	0.00	0.00
8	1.01	1.28	0.16	0.00	0.03	0.29	24	0.00	0.54	0.86	2.03	0.00	0.09	40	0.00	0.03	0.02	0.00	0.01	0.00
9	0.03	0.30	0.22	0.01	0.00	2.37	25	0.00	0.09	0.94	0.00	0.28	0.34	41	0.07	0.01	0.00	0.04	0.00	0.00
10	0.00	0.42	1.11	0.00	0.00	1.25	26	0.00	0.09	0.38	0.07	0.12	0.07	42	0.00	0.00	0.03	0.00	0.03	0.00
11	0.00	0.06	0.99	0.02	6.46	0.07	27	0.00	2.98	0.37	0.26	0.14	0.07	43	0.00	0.00	0.00	0.00	0.00	0.00
12	0.00	0.27	0.08	0.12	0.11	1.36	28	0.00	0.00	0.38	0.20	0.08	0.22	44	0.00	0.02	0.00	0.03	0.00	0.00
13	0.00	0.00	0.00	4.37	3.60	0.19	29	0.00	0.00	0.38	0.02	0.15	0.10	45	0.00	0.00	0.00	0.00	0.00	0.00
14	0.00	1.63	0.00	0.81	0.33	0.61	30	0.49	0.00	0.06	0.15	0.18	0.11	46	0.00	0.00	0.00	0.00	0.00	0.00
15	0.00	0.00	0.03	1.76	0.37	0.64	31	0.24	0.02	0.00	0.10	0.61	0.03	47	0.00	0.00	0.00	0.00	0.00	0.00
16	0.03	0.14	0.02	0.92	2.62	0.31	32	0.00	0.81	0.00	0.40	0.11	0.09	48	0.00	0.00	0.00	0.03	0.00	0.00

TABLE XII. The same as in Table VI but for OMC on ^{130}Xe to states in ^{130}I.

Bin No.	$W(J^\pi)/W_{\rm tot}(\%)$						Bin No.	$W(J^\pi)/W_{\rm tot}(\%)$						Bin No.	$W(J^\pi)/W_{\rm tot}(\%)$					
	0^+	1^+	2^+	1^-	2^-	Others		0^+	1^+	2^+	1^-	2^-	Others		0^+	1^+	2^+	1^-	2^-	Others
1	0.00	0.56	0.73	0.01	2.25	1.88	17	0.00	0.21	1.12	0.01	0.44	0.22	33	0.07	0.04	0.00	0.04	0.00	0.03
2	0.01	0.49	0.78	0.03	0.00	0.87	18	0.00	3.03	0.73	0.02	0.74	0.55	34	0.00	0.06	0.01	0.01	0.02	0.06
3	0.00	2.02	4.81	0.02	0.00	1.86	19	0.00	0.53	1.42	1.95	0.00	0.42	35	0.01	0.02	0.02	0.00	0.00	0.00
4	0.05	0.39	0.00	0.02	3.73	1.66	20	0.00	0.77	0.96	0.38	0.48	0.16	36	0.00	0.09	0.05	0.03	0.00	0.01
5	0.00	2.14	0.35	0.18	0.36	0.43	21	0.05	0.35	0.43	0.05	0.16	0.34	37	0.00	0.02	0.02	0.00	0.03	0.00
6	0.00	0.34	0.03	2.25	0.01	0.41	22	0.00	0.10	0.99	0.04	0.01	0.08	38	0.00	0.00	0.02	0.01	0.00	0.00
7	0.70	0.06	0.62	2.80	1.13	0.56	23	0.00	0.77	0.18	0.13	0.00	0.02	39	0.00	0.00	0.00	0.00	0.00	0.00
8	0.00	0.05	0.00	1.41	2.78	1.34	24	0.00	1.60	0.78	0.33	0.10	0.09	40	0.03	0.00	0.00	0.03	0.00	0.00
9	0.00	0.00	0.26	1.27	0.41	1.30	25	0.00	0.01	0.00	0.40	0.51	0.36	41	0.00	0.00	0.00	0.00	0.00	0.00
10	0.00	0.06	1.07	0.87	0.38	2.04	26	0.00	0.00	0.28	0.23	0.43	0.03	42	0.00	0.00	0.00	0.00	0.00	0.00
11	0.00	0.00	0.02	1.40	2.88	1.15	27	0.00	0.01	0.15	0.51	0.13	0.03	43	0.00	0.00	0.00	0.00	0.00	0.00
12	0.00	0.05	0.02	1.70	0.27	0.84	28	0.00	0.68	0.00	0.10	0.54	0.06	44	0.00	0.00	0.00	0.00	0.00	0.00
13	0.00	1.69	0.02	0.86	0.69	2.16	29	0.00	0.05	0.00	0.09	0.03	0.06	45	0.00	0.00	0.00	0.00	0.00	0.00
14	0.00	0.61	0.02	0.97	0.16	1.81	30	0.65	0.00	0.02	0.00	0.00	0.11	46	0.00	0.00	0.00	0.00	0.00	0.00
15	0.10	0.70	0.05	0.09	0.30	0.74	31	0.00	0.07	0.00	0.47	0.07	0.02	47	0.00	0.00	0.00	0.00	0.00	0.00
16	0.00	0.01	0.11	2.95	0.81	1.32	32	0.00	0.01	0.00	0.00	0.10	0.01	48	0.00	0.01	0.00	0.00	0.00	0.00

TABLE XIII. The same as in Table VI but for OMC on ^{136}Ba to states in ^{136}Cs.

Bin No.	$W(J^\pi)/W_{\rm tot}(\%)$						Bin No.	$W(J^\pi)/W_{\rm tot}(\%)$						Bin No.	$W(J^\pi)/W_{\rm tot}(\%)$					
	0^+	1^+	2^+	1^-	2^-	Others		0^+	1^+	2^+	1^-	2^-	Others		0^+	1^+	2^+	1^-	2^-	Others
1	0.00	1.12	0.39	0.00	2.31	0.95	18	0.00	0.54	1.72	1.92	1.30	0.92	35	0.00	0.02	0.04	0.00	0.00	0.05
2	0.00	0.00	0.61	0.03	0.00	1.58	19	1.11	2.62	0.62	0.08	0.00	0.36	36	0.00	0.05	0.01	0.00	0.00	0.00
3	0.00	2.45	0.25	0.02	0.00	0.31	20	0.00	0.91	1.63	0.02	0.02	0.14	37	0.00	0.05	0.02	0.00	0.00	0.00
4	0.00	0.10	5.35	0.02	0.02	2.42	21	0.00	0.72	0.66	0.02	0.00	0.34	38	0.00	0.00	0.03	0.01	0.00	0.00
5	0.00	2.46	0.00	0.06	3.66	1.36	22	0.01	0.17	0.70	0.01	0.00	0.04	39	0.00	0.00	0.00	0.01	0.00	0.00
6	0.00	0.33	0.43	1.21	0.01	0.38	23	0.00	1.83	1.19	0.04	0.01	0.06	40	0.01	0.00	0.00	0.01	0.00	0.00
7	0.00	0.00	0.03	2.78	0.01	0.20	24	0.00	0.46	0.30	0.79	0.00	0.06	41	0.48	0.00	0.00	0.00	0.00	0.00
8	0.00	0.02	0.35	2.17	1.96	1.06	25	0.00	0.03	0.05	0.11	0.07	0.34	42	0.00	0.00	0.00	0.00	0.00	0.00
9	0.00	0.00	0.00	1.03	2.77	1.09	26	0.00	0.01	0.35	0.28	0.53	0.10	43	0.00	0.00	0.00	0.00	0.00	0.00
10	0.00	0.00	0.20	1.81	0.38	1.83	27	0.00	0.84	0.00	0.49	0.56	0.05	44	0.00	0.00	0.00	0.00	0.00	0.00
11	0.00	0.05	1.31	1.33	1.16	1.93	28	0.00	0.00	0.00	0.13	0.17	0.11	45	0.00	0.00	0.00	0.00	0.00	0.00
12	0.00	0.00	0.02	1.69	2.01	1.39	29	0.00	0.01	0.00	0.00	0.40	0.10	46	0.00	0.00	0.00	0.00	0.00	0.00
13	0.00	0.20	0.01	0.37	0.30	0.64	30	0.00	0.02	0.00	0.46	0.05	0.02	47	0.00	0.00	0.00	0.00	0.00	0.00
14	0.01	1.31	0.00	1.67	0.55	3.24	31	0.00	0.00	0.00	0.01	0.00	0.02	48	0.00	0.00	0.00	0.00	0.00	0.00
15	0.00	0.04	0.01	0.06	0.28	0.25	32	0.00	0.01	0.00	0.05	0.13	0.01	49	0.00	0.01	0.00	0.00	0.00	0.00
16	0.04	0.06	0.02	3.04	0.93	1.20	33	0.04	0.01	0.00	0.00	0.02	0.02	50	0.00	0.00	0.00	0.00	0.00	0.00
17	0.00	0.26	0.07	0.01	0.10	1.00	34	0.00	0.08	0.02	0.00	0.00	0.03	51	0.01	0.00	0.00	0.00	0.00	0.00

[1] J. Suhonen and O. Civitarese, Phys. Rep. **300**, 123 (1998).
[2] D. Zinatulina, V. Brudanin, V. Egorov, C. Petitjean, M. Shirchenko, J. Suhonen, and I. Yutlandov, Phys. Rev. C **99**, 024327 (2019).
[3] H. Ejiri, J. Suhonen, and K. Zuber, Phys. Rep. **797**, 1 (2019).
[4] H. Ejiri, Phys. Rep. **338**, 265 (2000).
[5] D. F. Measday, Phys. Rep. **354**, 243 (2001).
[6] M. Kortelainen and J. Suhonen, Europhys. Lett. **58**, 666 (2002).
[7] M. Kortelainen and J. Suhonen, Nucl. Phys. A **713**, 501 (2003).
[8] M. Kortelainen and J. Suhonen, J. Phys. G: Nucl. Part. Phys. **30**, 2003 (2004).
[9] E. Kolbe, K. Langanke, and P. Vogel, Phys. Rev. C **50**, 2576 (1994).
[10] B. L. Johnson *et al.*, Phys. Rev. C **54**, 2714 (1996).
[11] T. P. Gorringe *et al.*, Phys. Rev. C **60**, 055501 (1999).
[12] T. Siiskonen, J. Suhonen, and M. Hjorth-Jensen, J. Phys. G: Nucl. Part. Phys. **25**, L55 (1999).
[13] T. Siiskonen, M. Hjorth-Jensen, and J. Suhonen, Phys. Rev. C **63**, 055501 (2001).
[14] N. Auerbach and B. A. Brown, Phys. Rev. C **65**, 024322 (2002).
[15] F. Šimkovic, G. Pantis, J. D. Vergados, and A. Faessler, Phys. Rev. C **60**, 055502 (1999).
[16] T. P. Gorringe *et al.*, Phys. Rev. Lett. **72**, 3472 (1994).
[17] G. Jonkmans, S. Ahmad, D. S. Armstrong, G. Azuelos, W. Bertl, M. Blecher, C. Q. Chen, P. Depommier, B. C. Doyle *et al.*, Phys. Rev. Lett. **77**, 4512 (1996).
[18] D. Gazit, Phys. Lett. B **666**, 472 (2008).
[19] L. E. Marcucci, A. Kievsky, S. Rosati, R. Schiavilla, and M. Viviani, Phys. Rev. Lett. **108**, 052502 (2012).
[20] V. Brudanin *et al.*, Nucl. Phys. A **587**, 577 (1995).
[21] T. Siiskonen, J. Suhonen, V. A. Kuz'min, and T. V. Tetereva, Nucl. Phys. A **635**, 446 (1998); **651**, 437(E) (1999).
[22] T. Siiskonen, J. Suhonen, and M. Hjorth-Jensen, Phys. Rev. C **59**, R1839 (1999).
[23] T. Gorringe and H. W. Fearing, Rev. Mod. Phys. **76**, 31 (2004).
[24] J. Suhonen, *From Nucleons to Nucleus: Concepts of Microscopic Nuclear Theory* (Springer, Berlin, 2007).
[25] D. R. Bes, O. Civitarese, and J. Suhonen, Phys. Rev. C **86**, 024314 (2012).
[26] O. Civitarese and J. Suhonen, Phys. Rev. C **89**, 044319 (2014).
[27] H. Ejiri, Phys. Rep. **38**, C85 (1978).
[28] L. Jokiniemi and J. Suhonen, Phys. Rev. C **96**, 034308 (2017).
[29] L. Jokiniemi, J. Suhonen, H. Ejiri, and I. H. Hashim, Phys. Lett. B **794**, 143 (2019).
[30] I. H. Hashim, H. Ejiri, T. Shima, K. Takahisa, A. Sato, Y. Kuno, K. Ninomiya, N. Kawamura, and Y. Miyake, Phys. Rev. C **97**, 014617 (2018).
[31] L. Jokiniemi, H. Ejiri, D. Frekers, and J. Suhonen, Phys. Rev. C **98**, 024608 (2018).
[32] J. Suhonen, Front. Phys. **5**, 55 (2017).
[33] M. Morita and A. Fujii, Phys. Rev. **118**, 606 (1960).
[34] H. Primakoff, Rev. Mod. Phys. **31**, 802 (1959).
[35] K. W. Ford and J. G. Wills, Nucl. Phys. **35**, 295 (1962).
[36] H. Ejiri, Front. Phys. **7**, 30 (2019).
[37] M. L. Goldberger and S. B. Treiman, Phys. Rev. **111**, 354 (1958).
[38] J. Suhonen, T. Taigel, and A. Faessler, Nucl. Phys. A **486**, 91 (1988).
[39] F. Šimkovic, V. Rodin, A. Faessler, and P. Vogel, Phys. Rev. C **87**, 045501 (2013).
[40] A. Bohr and B. R. Mottelson, *Nuclear Structure* (Benjamin, New York, 1969), Vol. I.
[41] K. Holinde, Phys. Rep. **68**, 121 (1981).
[42] J. Suhonen, Nucl. Phys. A **563**, 205 (1993).
[43] J. Suhonen, Nucl. Phys. A **700**, 649 (2002).
[44] P. Sarriguren, Phys. Rev. C **86**, 034335 (2012).